ATHEROGENIC DYSLIPIDEMIA AND INSULIN RESISTANCE AS DRIVERS OF EARLY LIVER AND KIDNEY INJURY IN EXPERIMENTAL METABOLIC SYNDROME

Nigora F. Abdukhalikova, Bakhtiyar U. Iriskulov, Alisher Kh. Rakhmonov
Tashkent State Medical University (Tashkent, Uzbekistan)
dr.ali.fl@mail.ru

Abstract. Background: *Metabolic syndrome (MetS) is a systemic cardiometabolic disorder that increases the risk of target-organ damage, including metabolic dysfunction–associated steatotic liver disease (MASLD) and early kidney injury. However, integrated experimental evidence linking metabolic derangements with parallel hepatic and renal impairment remains limited.*

Materials and methods: *Male rats were allocated to control and MetS groups. MetS was induced by high-fat loading combined with fructose supplementation for 12 weeks. Serum metabolic and organ injury markers were assessed, including lipid abnormalities and indices of renal dysfunction (urea, creatinine, globulins). Urinalysis included specific gravity, pH, total protein, albumin, nitrogen metabolites, and electrolytes (Na, K). Liver and kidney tissues were examined histologically, and liver damage was quantified by morphometric analysis (steatosis area, lipid-laden hepatocytes, mononuclear infiltration).*

Results: *MetS animals developed significant renal dysfunction characterized by azotemia, marked proteinuria/albuminuria, reduced urinary concentrating capacity, urinary acidification, and electrolyte imbalance consistent with tubular transport dysregulation. Histology demonstrated preserved renal architecture in controls and focal early glomerular and tubular alterations in MetS rats. In parallel, MetS induced pronounced liver injury with macro- and microvesicular steatosis, inflammatory infiltration, and morphometrically confirmed expansion of steatotic areas and lipid-laden hepatocytes.*

Conclusions: *Twelve-week experimental MetS results in concurrent hepatic steatosis and early renal injury, supporting the concept of a cardiometabolic continuum. Combined biochemical, urinary, and morphometric markers provide a robust platform for mechanistic studies and evaluation of nephro- and hepatoprotective interventions in MetS.*

Keywords: *metabolic syndrome; kidney injury; proteinuria; albuminuria; azotemia; hepatic steatosis; morphometry; rat model.*

Metabolic syndrome (MetS) comprises a constellation of interrelated metabolic abnormalities—visceral obesity, insulin resistance/hyperglycemia, arterial hypertension, and atherogenic dyslipidemia—that substantially increases the risk of cardiovascular complications and contributes to an elevated systemic “cardiorenometabolic” risk burden. In recent years, MetS has been recognized as an independent predictor of chronic kidney disease (CKD), being associated with an accelerated decline in glomerular filtration rate and a higher prevalence of albuminuria even in the absence of overt diabetes mellitus [5]. Meta-analytic evidence further supports a robust association between MetS and an increased risk of renal dysfunction and CKD, including unfavorable eGFR trajectories and progression to end-stage kidney disease [5]. Importantly, the magnitude of renal risk increases with the number of MetS components, as the combination of visceral adiposity, hypertension, and dyslipidemia exerts additive adverse effects on renal microcirculation and glomerular filtration [3]. Albuminuria, including low-grade albuminuria, is therefore considered an early clinically meaningful marker of metabolically mediated kidney injury and, concurrently, an indicator of endothelial dysfunction and heightened cardiovascular risk [2].

Key pathogenetic mechanisms of kidney injury in metabolic syndrome (MetS)

1. **Hemodynamic alterations: hyperfiltration and RAAS activation.** In the early stages of metabolic syndrome, glomerular hyperfiltration frequently develops and is accompanied by increased intraglomerular pressure and activation of the renin–angiotensin–aldosterone system (RAAS). These changes promote podocyte injury, increase permeability of the filtration barrier, and lead to albuminuria as an early marker of glomerular dysfunction [6].

2. **Visceral and perirenal obesity.** Visceral adipose tissue—particularly perirenal fat and renal sinus fat—acts as an active source of pro-inflammatory cytokines, adipokine imbalance, and an increased flux of free fatty acids. This milieu contributes to endothelial dysfunction, enhanced oxidative stress, and the maintenance of local inflammatory responses within renal tissue [9].

3. **Lipotoxicity and impaired renal energy metabolism.** Atherogenic dyslipidemia and insulin resistance facilitate intrarenal lipid accumulation, including deposition within tubular epithelial cells. Lipid overload induces endoplasmic reticulum stress, mitochondrial dysfunction, and hypoxia-related reactive oxygen species generation, thereby serving as a major driver of tubulointerstitial injury and fibrosis [1].

4. **Chronic low-grade inflammation and oxidative stress.** Metabolic syndrome sustains systemic “metabolic inflammation” and excessive ROS production, which damages the glomerular endothelium and activates pro-fibrotic signaling pathways (including the TGF-β cascade). Consequently, interstitial fibrosis progresses and glomerular filtration rate declines, providing a mechanistic basis for CKD development and progression [7].

Materials and Methods.

Study Design

This study was designed as a controlled experimental animal study with parallel group allocation.

Animals

Initially, 20 male rats were enrolled in the study. During the experimental period, four animals were excluded due to technical reasons unrelated to the study protocol (e.g., tissue processing artifacts). The final analysis was performed on 16 rats, which were randomly assigned to the control (n = 8) and experimental (n = 8) groups. Group allocation was performed using a computer-generated randomization sequence with a 1:1 allocation ratio. Allocation concealment was maintained by assigning coded identifiers to each animal. Histological and morphometric analyses were performed by an investigator blinded to group allocation. The MetS model was established in male rats to minimize hormonal variability associated with the estrous cycle.

All animal procedures were conducted in accordance with applicable international guidelines and the EU Directive 2010/63/ EU on the protection of animals used for scientific purposes. The protocol was approved by the Local Ethics Committee of Tashkent Medical Academy (now Tashkent State Medical University) (Protocol No. 6, June 25, 2025).

Animals were housed under standard vivarium conditions with a 12-hour light-dark cycle and free access to food and water.

Diet

Rats in the control group received a standard laboratory diet with an energy content of 280–310 kcal per 100 g of feed. The diet consisted of 18–22 % protein, 4–6 % fat, 55–65 % digestible carbohydrates, 4–6 % fiber, 5–7 % ash, and 10–12 % moisture.

The mineral composition included calcium (0.8–1.2 %), phosphorus (0.6–0.9%), sodium chloride (0.3–0.5 %), magnesium (0.2–0.3 %), potassium (0.6–1.0 %), iron (100–200 mg/kg), zinc (50–100 mg/kg), copper (8–15 mg/kg), manganese (70–150 mg/kg), selenium (0.1–0.3 mg/kg), and iodine (0.5–2 mg/kg).

The vitamin content comprised vitamin A (4,000–10,000 IU/kg), vitamin D_3 (800–1,500 IU/kg), vitamin E (30–80 mg/kg), vitamin K (1–3 mg/kg), and a B-complex vitamin mixture (B_1, B_2, niacin, B_6, pantothenic acid, folic acid, biotin, and B_{12}) within recommended concentrations.

The main feed ingredients included cereals (corn, wheat, oats), soybean meal or protein concentrates, fish meal or meat-and-bone meal, vegetable oils, dried grass meal, and a vitamin–mineral premix.

Rats in the experimental group received a high-fat diet combined with fructose supplementation to induce metabolic syndrome. The diet was characterized by an increased fat content compared to the standard laboratory chow, while drinking water was supplemented with fructose throughout the experimental period. The dietary intervention was maintained for 12 weeks.

Experimental Diet Protocol

Rats in the experimental group were administered melted sheep mesenteric fat intragastrically via a metal gavage needle prior to feeding. The fat was maintained in a water bath at 38–40 °C and delivered at a dose of 1 g per 100 g of body weight. The procedure was performed once daily throughout the experimental period. One hour after fat administration, animals were provided with the standard laboratory diet. The procedure was performed by an experienced operator to minimize stress and discomfort to the animals.

As a drinking fluid, the experimental group received 10 % fructose solution ad libitum throughout the experimental period.

Rat Euthanasia and Sample Collection

At the end of the 12-week experimental period, rats were fasted for 12 hours and anesthetized using short-term inhalation anesthesia. Blood samples were collected by direct puncture of the jugular vein into sterile tubes and subsequently centrifuged at 3000 rpm for 10 minutes to obtain serum. The collected serum samples were stored at −20 °C until further biochemical analysis.

Liver and Kidney Histology

Liver and kidney specimens were fixed in 10% neutral buffered formalin for at least 24 h and subsequently processed using standard paraffin-embedding procedures. Tissues were dehydrated through a graded ethanol series (70–100%), cleared in xylene, and infiltrated with paraffin at 60 °C. Paraffin sections (5–7 μm) were cut on a microtome, mounted on positively charged glass slides, and dried at 37–42 °C.

Sections were stained with hematoxylin and eosin (H&E) according to standard protocols and examined using a Leica DM IL LED microscope. Quantitative image analysis was performed in Fiji. For each group, randomly selected non-overlapping fields of view were analyzed, and images were saved in TIFF format for subsequent processing. Quantification was conducted by calculating the percentage of stained area relative to the total tissue area.

Mononuclear cell infiltration in the liver parenchyma was quantified on ×20 images. For each animal, five randomly selected fields were analyzed. Individual mononuclear cells were counted manually using the “Multi-point” tool in Fiji, with a point placed on each nucleus to ensure reproducibility; results were recorded in the ROI Manager for documentation.

Counting of lipid-laden cells. Lipid-laden cells, including hepatocytes exhibiting cytoplasmic vacuolization, were identified in H&E-stained sections based on the presence of cytoplasmic vacuoles. Counts were performed manually on ×20 images. For each animal, five randomly selected hepatic fields were analyzed. Cells were counted using the Fiji “Multi-point” tool, with points placed on each vacuolated cell; data were stored in the ROI Manager for verification and documentation. Final results were expressed as the mean number of lipid-laden cells per field of view.

Biochemical Analysis

The following parameters were measured: lipid profile, including total cholesterol (TC), low density lipoprotein cholesterol (LDL-C), high-density lipoprotein cholesterol (HDL-C), and triglycerides (TG), urea, creatinine, globulin which were determined using commercially available rat-specific assay kits (Vector-Best, Russia). Blood glucose and insulin levels were also measured using rat-specific kits (Vector-Best, Russia). Insulin resistance (IR) was assessed using the homeostasis model assessment (HOMA-IR) according to the following formula [8].

HOMA-IR = (fasting glucose (mmol/L) × fasting insulin (μIU/mL)) / 22.5

Serum levels of alanine aminotransferase (ALT), aspartate aminotransferase (AST), alkaline phosphatase, gamma-glutamyltransferase (GGT), total protein, albumin, and bilirubin were measured using commercial assay kits (Vector-Best, Russia).

Statistical Analysis

Data are presented as mean ± standard deviation (SD). Normality was assessed using the Shapiro–Wilk test. Homogeneity of variances was evaluated using Levene's test. Between-group comparisons were performed using an independent samples t-test. Effect sizes (Cohen's d) were calculated where appropriate. Where appropriate, 95% confidence intervals (CI) were calculated. Given the limited sample size (n = 16) and potential deviations from normal distribution, correlations between metabolic and histomorphometric parameters were assessed using Spearman's rank correlation coefficient (ρ) All tests were two-tailed, and a p-value < 0.05 was considered statistically significant. Statistical analyses were performed using IBM SPSS Statistics (version 20.0, IBM Corp., Armonk, NY, USA) and Jamovi (version 2.6.44; The Jamovi Project, Sydney, Australia).

Results.

Development of Obesity and Increase in Mesenteric Fat Index in Experimental MetS

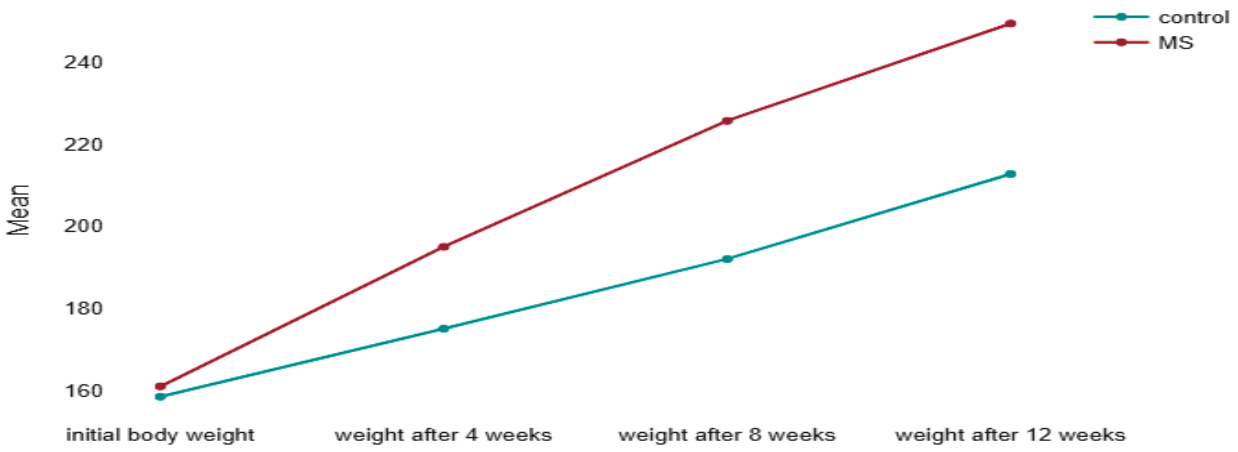


Figure 1. Time-dependent changes in body weight in control and MetS groups over the 12-week experimental period. Values are presented as mean ± SD; p < 0.001 vs. control

Rats in the MetS group showed a significantly greater body weight gain compared with controls from week 4 onward ($p < 0.001$). By week 12, weight increased by approximately 60% in the MetS group versus 35% in controls, confirming successful induction of obesity (Fig. 1).

Metabolic and Biochemical Alterations Associated with Liver Injury in the Experimental MetS Model

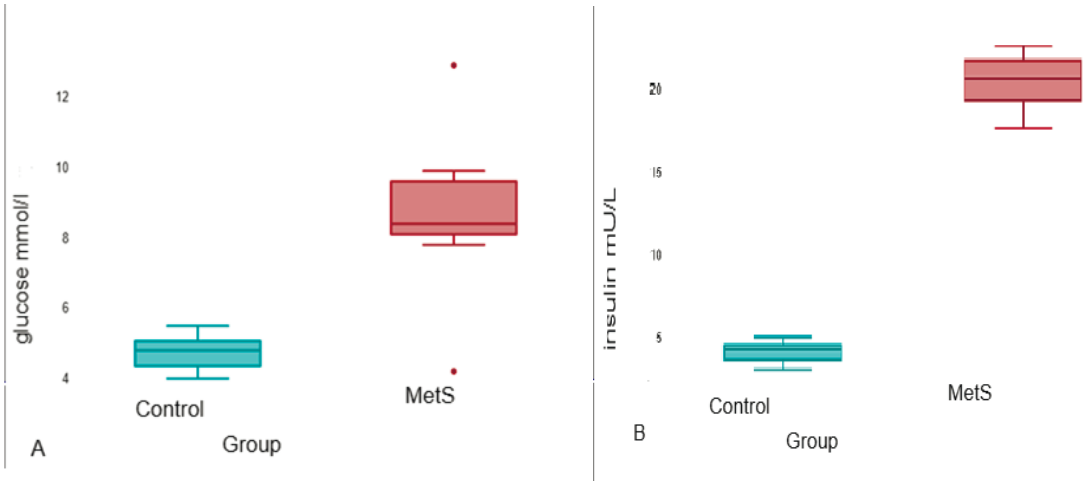


Figure 2. Blood glucose (A) and insulin (B) concentrations in control animals and rats with experimentally induced MetS after 12 weeks ($p < 0.001$)

MetS rats exhibited significantly elevated blood glucose levels compared with controls ($p < 0.001$), accompanied by increased insulin resistance, as reflected by an increase in HOMA-IR from 0.87 to 7.86 ($p < 0.001$), representing an approximately ninefold increase.

Table 1.

Lipid profile parameters in control and MetS groups

Parameter (mmol/L)	Control (n = 8)	MetS (n = 8)	p value
Cholesterol	1.21 ± 0.22	2.45 ± 0.47	< 0.001
LDL-C	1.22 ± 0.17	1.98 ± 0.32	< 0.001
HDL-C	0.94 ± 0.17	0.80 ± 0.15	0.096
Triglycerides	1.73 ± 0.36	3.58 ± 0.57	< 0.001

MetS animals exhibited marked atherogenic dyslipidemia, characterized by significantly increased total cholesterol, LDL-C, and triglyceride levels (all $p < 0.001$), along with a non significant trend toward reduced HDL-C concentrations ($p = 0.096$).

Table 2.

Liver biochemical markers in control and MetS groups

Parameter	Control (n = 8)	MetS (n = 8)	P value
Alanine aminotransferase (ALT), U/L	54.74 ± 4.23	133.75 ± 14.69	< 0.001
Aspartate aminotransferase (AST), U/L	82.89 ± 9.81	149.78 ± 27.82	< 0.001
Alkaline phosphatase (ALP), U/L	276.16 ± 46.27	539.99 ± 84.01	< 0.001
Gamma-glutamyltransferase (GGT), U/L	5.14 ± 0.82	19.79 ± 4.15	< 0.001
Total protein, g/L	72.15 ± 2.57	52.48 ± 9.72	< 0.001
Albumin, g/L	33.91 ± 1.13	24.36 ± 1.04	< 0.001
Total bilirubin, µmol/L	1.27 ± 0.24	4.05 ± 0.70	< 0.001

After 12 weeks of MetS induction, rats showed significant biochemical evidence of liver injury. ALT and AST activities increased 2.4-fold and 1.8-fold, respectively ($p < 0.001$), indicating marked hepatocellular damage. Alkaline phosphatase and γ-glutamyltransferase activities were elevated (≈2-fold and ≈4-fold; $p < 0.001$), reflecting a pronounced cholestatic component. Total protein and albumin levels decreased by 27% and 28% ($p < 0.001$), while total bilirubin increased more than

threefold ($p < 0.001$), confirming impaired hepatic synthetic function and mixed hepatocellular–cholestatic injury [9].

Table 3.

Biochemical markers of renal function in control and metabolic syndrome (MetS) rats after 12 weeks

Parameter	Control (n = 8)	MetS (n = 8)	P value
Globulin, g/L	29.28 ± 4.48	37.28 ± 4.75	0.0038
Urea, mmol/L	5.15 ± 0.83	8.81 ± 1.69	< 0.001
Creatinine, µmol/L	47.23 ± 8.17	71.89 ± 12.17	< 0.001

After 12 weeks of MetS induction, significant changes in biochemical markers indicative of renal involvement were observed. In the MetS group, serum urea levels were markedly higher than in controls ($p < 0.001$), and creatinine concentrations were similarly increased ($p < 0.001$). In addition, globulin levels were significantly elevated ($p = 0.0038$), which may reflect activation of an inflammatory component in MetS.

Taken together, these alterations indicate the development of azotemia and suggest a likely reduction in glomerular filtration and/or renal excretory function, consistent with the concept of MetS-associated kidney injury as an early manifestation of the cardiorenometabolic continuum. The increase in globulins further supports the presence of chronic low-grade systemic inflammation characteristic of MetS and may indirectly reflect immunoinflammatory activation contributing to microvascular and tubulointerstitial changes in renal tissue. Overall, the findings confirm that MetS is associated not only with metabolic disturbances but also with early signs of renal dysfunction accompanied by an inflammatory component, thereby increasing the risk of nephropathy progression with prolonged disease duration.

Table 4.

Urinalysis parameters in control and metabolic syndrome (MetS) rats after 12 weeks

Parameter	Control (n = 8)	MetS (n = 8)	P value
Relative volume (mL)	4.39 ± 0.43	7.22 ± 0.46	< 0.0001
Specific gravity	1.0384 ± 0.0076	1.0104 ± 0.0050	< 0.0001
pH	7.91 ± 0.41	6.39 ± 0.38	< 0.0001
Total protein (g/L)	0.036 ± 0.007	0.390 ± 0.055	< 0.0001
Albumin (mg/L)	4.82 ± 0.99	29.00 ± 5.17	< 0.0001
Uric acid (mmol/L)	0.82 ± 0.15	2.08 ± 0.31	< 0.0001
Creatinine (mmol/L)	5.81 ± 0.81	14.60 ± 1.92	< 0.0001
Urea (mmol/L)	52.53 ± 7.50	97.32 ± 16.09	< 0.0001
Sodium (Na), mmol/L	122.36 ± 17.14	81.71 ± 14.57	0.0002
Potassium (K), mmol/L	49.14 ± 9.19	91.31 ± 12.31	< 0.0001

In the MetS group, markedly pronounced proteinuria/albuminuria was observed: total urinary protein increased approximately 11-fold and urinary albumin increased approximately 6-fold (both $p < 0.0001$), consistent with glomerular filtration barrier injury and increased permeability, reflecting early MetS-associated kidney involvement. Urinary creatinine and urea levels were also significantly elevated ($p < 0.0001$), suggesting substantial disturbances in nitrogen metabolism and/or impaired renal excretory function (this interpretation would be further strengthened by concomitant serum creatinine/urea measurements and eGFR estimation). A reduction in urine specific gravity ($p < 0.0001$), together with a shift in urinary pH toward acidity ($p < 0.0001$), may indicate impaired concentrating ability and tubular dysfunction. The electrolyte profile showed decreased urinary Na^+ ($p = 0.0002$) and increased urinary K^+ ($p < 0.0001$), indicating dysregulation of tubular electrolyte

transport, which is typical of renal metabolic/inflammatory and hemodynamic stress in MetS (Table 4).

Histopathological Features of Hepatic and Renal Tissues in Experimentally Induced Steatosis

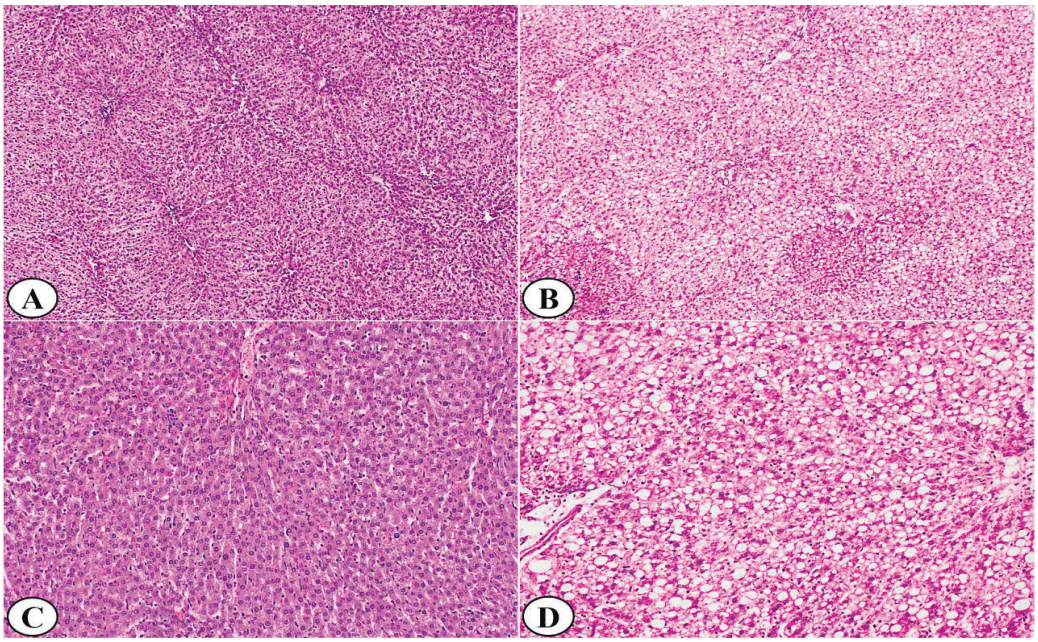


Figure 3. Representative photomicrographs of liver histology in the control (A, C) and experimental (B, D) groups at low (×10; A and B) and intermediate (×20; C and D) magnifications

At ×10 and ×20 magnifications, control livers preserved normal lobular architecture with well-defined central veins, radially arranged hepatocyte plates, and uniformly distributed sinusoids, with no evidence of steatosis, inflammation, necrosis, or fibrosis (Figure 3 A, C). In contrast, MetS livers exhibited marked architectural disruption characterized by trabecular disorganization, fragmented central veins, diffuse hepatocellular vacuolization, combined macro- and microvesicular steatosis, moderate mononuclear inflammatory infiltration, and focal early fibrotic changes predominantly in centrilobular and midzonal regions (Figure 3 B, D).

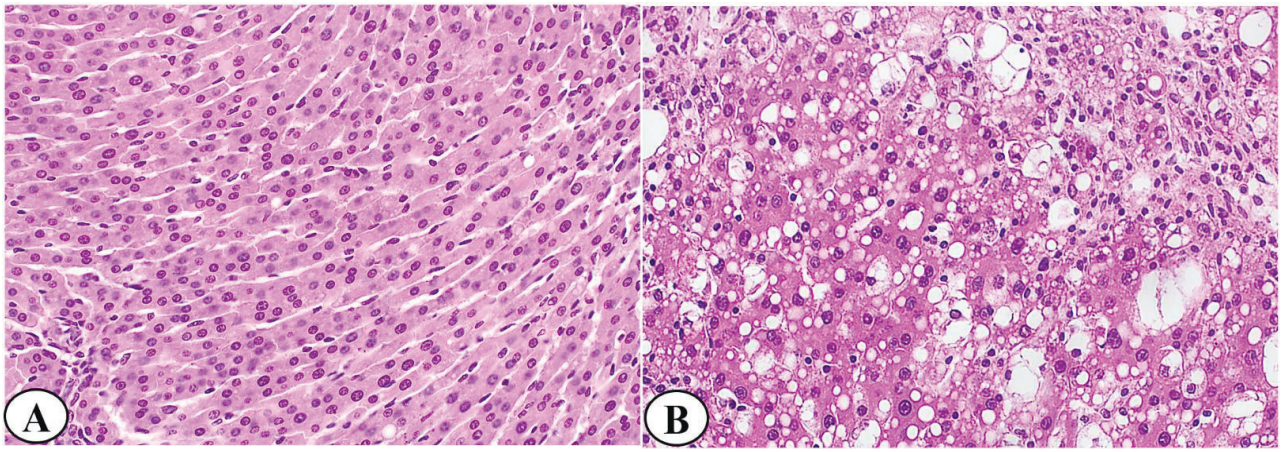


Figure 4. Representative photomicrographs of liver tissue from control (A) and MetS (B) groups at high magnification (×40)

At ×40 magnification, control livers displayed preserved hepatocellular architecture without steatosis or inflammation, whereas MetS livers exhibited pronounced macro- and microvesicular steatosis, hepatocyte vacuolization, nuclear degeneration, sinusoidal distortion, and moderate inflammatory infiltration, indicating progressive lipotoxic liver injury (Fig. 4.A, B).

After confirming the presence of steatosis in the experimental groups, a morphological assessment of the kidneys was performed to identify potential histological changes associated with hepatic lipid accumulation. This approach enables evaluation of whether steatosis induces secondary structural alterations in renal tissue and provides insight into the systemic consequences of disturbed lipid metabolism.

In the control group, renal histology demonstrated completely preserved cortical and medullary architecture with no pathological changes. Glomeruli displayed normal morphology; Bowman's capsule and Bowman's space were clearly delineated, and there was no evidence of sclerosis, congestion, or inflammatory changes. Proximal and distal tubules retained an intact epithelial lining (including preservation of the brush border), without dilation, necrosis, vacuolization, or casts; the interstitium and vascular structures showed no edema, fibrosis, or inflammatory infiltration, confirming overall renal structural integrity.

In the experimental group, the general cortico-medullary architecture was largely preserved; however, focal early alterations consistent with metabolic stress were observed. Most glomeruli remained free of sclerosis and destructive changes, yet some exhibited sporadic vesicular inclusions and mild hyperemia with dilated, congested capillary loops, which may reflect early microcirculatory and intracellular disturbances. Bowman's space and capsule remained preserved, without thickening or signs of inflammatory reaction (Fig. 5A, B).

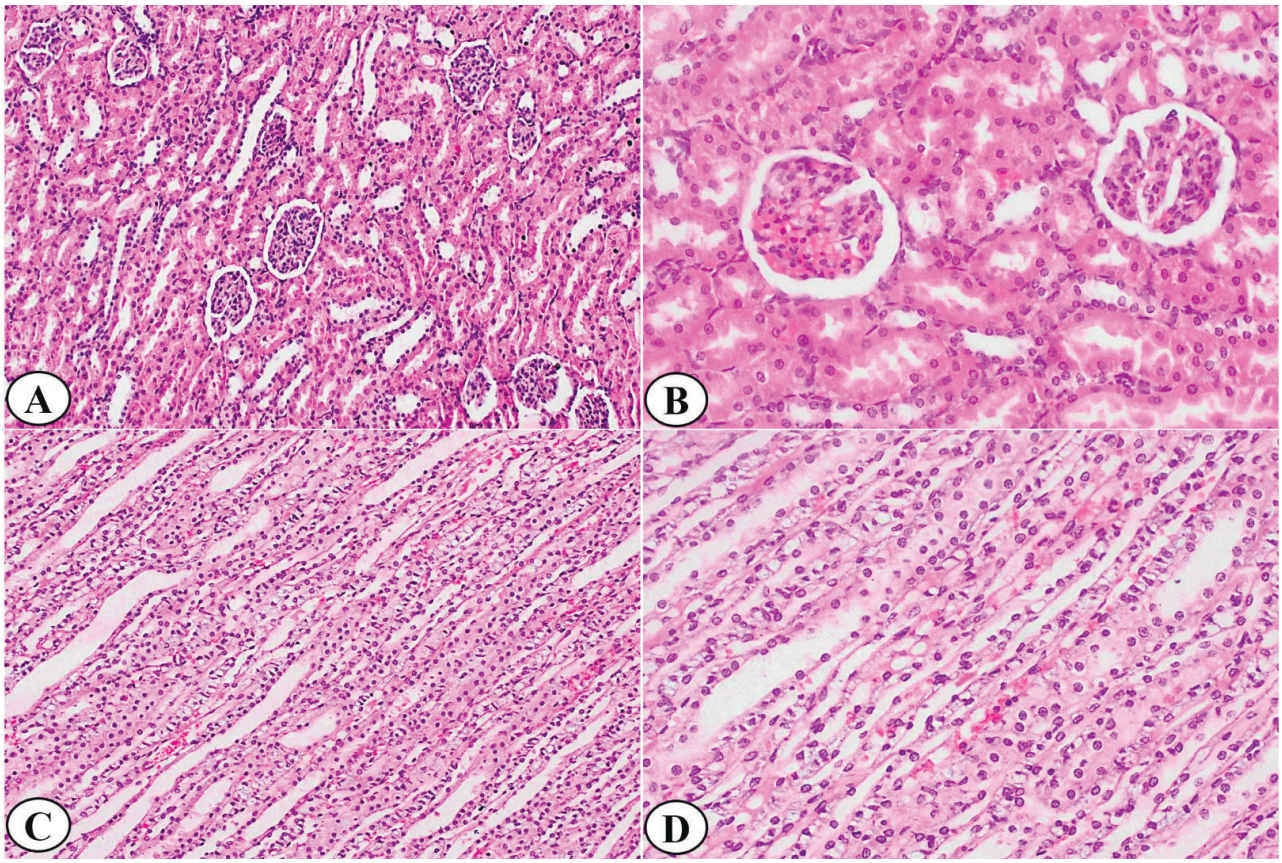


Figure 5. Representative photomicrographs of renal tissue from the experimental group at low (×10) and intermediate (×20) magnification. Panels A and B show the renal cortex, whereas panels C and D show the renal medulla

The tubular changes were focal and of moderate severity. In a subset of proximal and distal tubules, luminal dilatation with epithelial flattening/thinning was observed; in some proximal segments, partial loss of the brush border was noted. Occasional tubular epithelial cells showed cytoplasmic pallor and vacuolization, and sporadic desquamation into the tubular lumen was detected without evidence of overt necrosis. The medulla remained structurally preserved: collecting ducts and loops of Henle were orderly arranged, the interstitium showed no edema, fibrosis, or inflammatory infiltration, and vascular structures were patent with intact endothelium and minimal perivascular changes (Fig. 5C, D).

Overall, these findings are consistent with mild, focal tubular dysfunction accompanied by minimal glomerular involvement, compatible with metabolically induced renal injury in the setting of confirmed hepatic steatosis. Despite the presence of localized alterations (vesicular inclusions, mild glomerular hyperemia, and focal tubular epithelial changes), no features of advanced structural destruction of renal tissue were identified.

Morphometric Assessment of Hepatic and Renal Injury in an Experimental Model of Hepatic Steatosis.

A quantitative morphometric analysis was performed to objectively assess the severity of hepatic injury in the experimental model. Key parameters included the mean steatosis area within the liver parenchyma (Fig. 6A), the number of lipid-laden hepatocytes (Fig. 6B), and the degree of mononuclear cell infiltration (Fig. 6C).

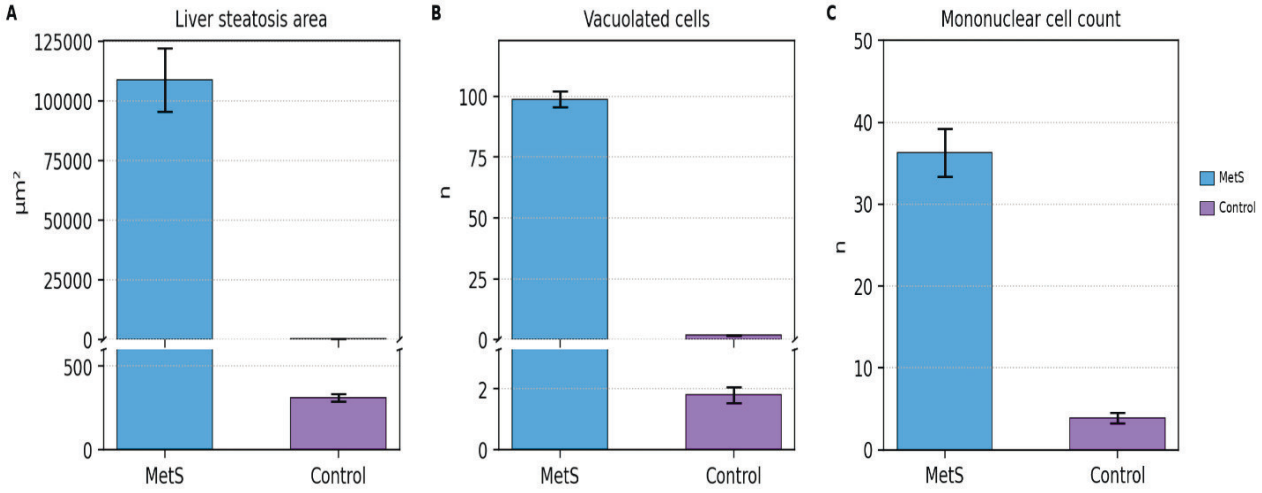


Figure 6. Morphometric assessment of the liver in control and MetS groups. A. Quantitative evaluation of hepatic steatosis area (µm² per standardized microscopic field). B. Number of vacuolated hepatocytes per microscopic field (×20). C. Quantitative evaluation of mononuclear cell infiltration in the liver parenchyma

Morphometric analysis revealed a marked increase in hepatic steatosis area in the experimental group compared with controls (108,884 ± 13,405.85 vs. 312 ± 23.14 µm²; $p < 0.0001$), indicating massive lipid accumulation within the liver parenchyma (Figure 6 A). The number of vacuolated hepatocytes was also significantly higher in the MetS group (98.8 ± 3.24 vs. 1.8 ± 0.25; $p < 0.0001$), reflecting pronounced cellular lipid overload (Figure 6 B). In addition, mononuclear cell infiltration was markedly increased (36.3 ± 2.89 vs. 3.9 ± 0.67; $p < 0.0001$), indicating activation of inflammatory processes in the liver (Figure 6 C).

Morphometric analysis of renal tissue included assessment of glomerular area, total glomerular count, and the number of vacuolated tubular epithelial cells (Figure 7). The mean glomerular area in the experimental group was 13,838.61 ± 899.40 µm², compared with 14,450.00 ± 1,568.50 µm² in controls, showing no significant between-group difference and indicating preservation of overall glomerular morphometric structure (Figure 7A). The total number of glomeruli also did not differ between groups (15.3 ± 2.23 in the experimental group vs 13.9 ± 1.95 in controls; Figure 7B), supporting stability of global glomerular cellularity.

In contrast, the number of glomeruli containing vacuolated cells was markedly higher in the experimental group (5.9 ± 0.43) than in controls (0.2 ± 0.13), and this difference was highly significant ($p < 0.0001$) (Figure 7B), suggesting focal glomerular involvement consistent with cellular lipid accumulation and/or early dystrophic changes. Quantification of vacuolated cells in renal tubules revealed pronounced between-group differences: the experimental group exhibited a substantially higher number of vacuolated tubular epithelial cells (95.8 ± 4.60) compared with the control group (5.4 ± 1.06; $p < 0.0001$) (Figure 7C).

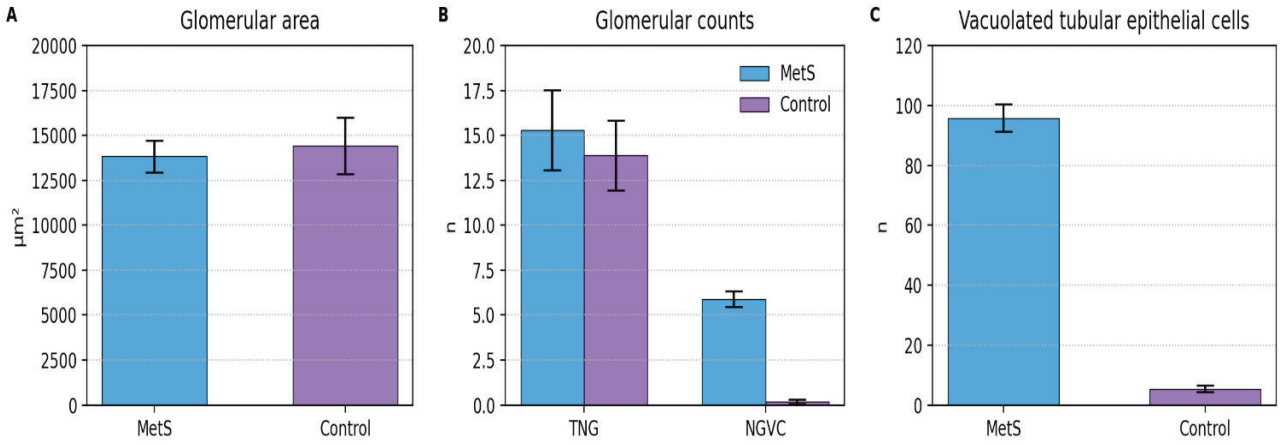


Figure 7. Morphometric assessment of the kidneys in the control (CG) and experimental (EG) groups: (A) mean glomerular area per field of view; (B) mean number of glomeruli per field of view, including the total number of glomeruli (TNG) and the number of glomeruli containing vacuolated cells (NGVC); (C) number of vacuolated tubular epithelial cells

These findings indicate that, in the setting of experimentally induced hepatic steatosis, the kidneys exhibit focal morphometric alterations in both glomeruli and tubules, while the overall renal architecture remains relatively preserved. To explore potential inter-organ interactions under metabolic stress, we performed a correlation analysis between hepatic steatosis area and renal morphometric indices of structural changes in the experimental animals (Figure 8).

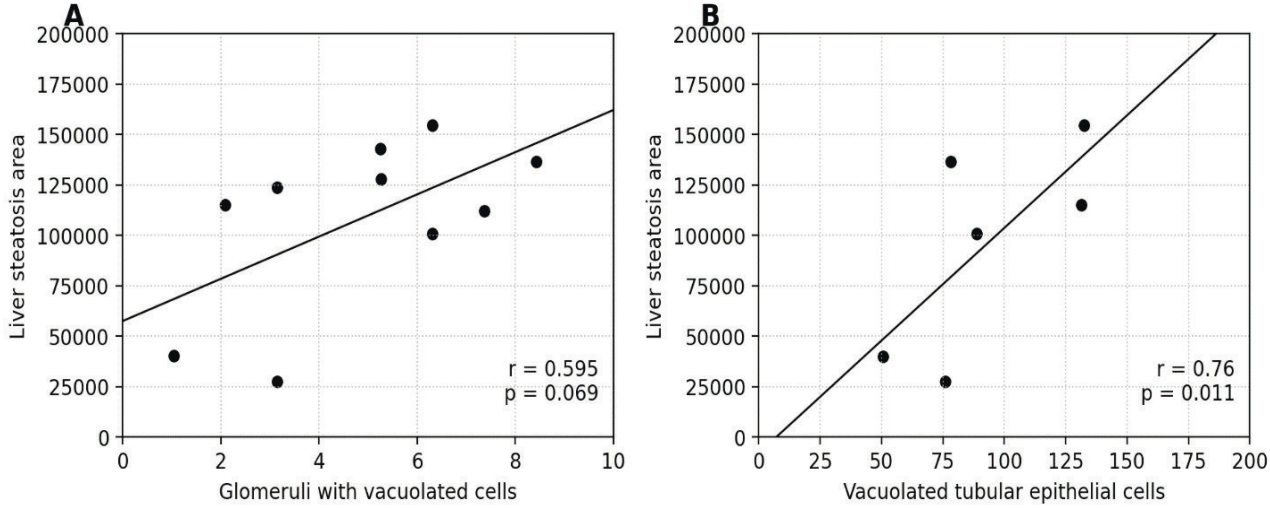


Figure 8. Correlation analysis of associations between renal morphometric features and the severity of hepatic steatosis in the experimental group (EG): (A) correlation between liver steatosis area and the number of glomeruli containing vacuolated cells; (B) correlation between liver steatosis area and the number of vacuolated tubular epithelial cells

Correlation analysis between renal morphometric indices and the severity of hepatic steatosis revealed associations that underscore the systemic nature of metabolic disturbances. In the experimental group, a positive trend was observed between liver steatosis area and the number of glomeruli containing vacuolated cells ($r = 0.595$; $p = 0.069$), suggesting a potential linkage between hepatocellular lipid accumulation and early glomerular alterations (Fig. 8A). A stronger and statistically significant correlation was identified between liver steatosis area and the number of vacuolated tubular epithelial cells ($r = 0.76$; $p = 0.011$) (Fig. 8B), indicating a close relationship between steatosis progression and structural remodeling of the tubular compartment.

Overall, these findings suggest that, in experimentally induced hepatic steatosis, quantitative changes are most pronounced in the liver, whereas the kidneys exhibit early focal morphometric signs of injury, predominantly at the tubular level. The presence of positive correlations between hepatic steatosis severity and indices of vacuolization in glomeruli and renal tubules further supports inter-organ coupling of metabolic injury and is consistent with the concept of systemic metabolic impact on target organs.

Conclusion. In this experimental model of metabolic syndrome, a constellation of findings consistent with MetS-associated kidney injury developed after 12 weeks, manifesting as a metabolically mediated nephropathy within the early cardiorenometabolic continuum. The significant increase in serum urea and creatinine indicates the development of azotemia and suggests a likely reduction in glomerular filtration and/or renal excretory function. Concurrently, marked proteinuria and albuminuria point to glomerular filtration barrier injury with increased permeability, whereas decreased urine specific gravity and a shift in urinary pH toward acidity reflect involvement of tubular and concentrating functions. Alterations in urinary electrolytes ($Na^+\downarrow$, $K^+\uparrow$) further support dysregulation of tubular electrolyte handling under conditions of metabolic and hemodynamic stress. Elevated globulin levels are consistent with activation of chronic low-grade systemic inflammation, a key pathogenetic component contributing to the progression of renal injury in MetS. Collectively, these data demonstrate that metabolic syndrome leads not only to hepatic and lipid abnormalities but also to early biochemical and urinary markers of renal dysfunction, underscoring the need for early renal monitoring and the development of pathogenetically targeted strategies to prevent nephropathy progression.

REFERENCES

1. Chae S. Y., Kim Y., Park C. W. Oxidative stress induced by lipotoxicity and renal hypoxia in diabetic kidney disease and possible therapeutic interventions: targeting the lipid metabolism and hypoxia //Antioxidants. – 2023. – T. 12. – №. 12. – C. 2083.

2. Claudel S. E., Verma A. Albuminuria in cardiovascular, kidney, and metabolic disorders: a state-of-the-art review //Circulation. – 2025. – T. 151. – №. 10. – C. 716-732.

3. dos Anjos Ribeiro Y., Franco A. C. B., da Silva L. S. Association between metabolic syndrome and chronic kidney disease in the Brazilian population, a cross-sectional analysis //Scientific Reports. – 2025.

4. Guerra Ruiz AR, et al. Measurement and clinical usefulness of bilirubin in liver disease. Adv Lab Med. 2021;2(3):352-372.

5. Li X. et al. The effect of metabolic syndrome and its individual components on renal function: a meta-analysis //Journal of clinical medicine. – 2023. – T. 12. – №. 4. – C. 1614.

6. Lin L. et al. Metabolic syndrome-related kidney injury: a review and update //Frontiers in endocrinology. – 2022. – T. 13. – C. 904001.

7. Masenga S. K. et al. Mechanisms of oxidative stress in metabolic syndrome //International journal of molecular sciences. – 2023. – T. 24. – №. 9. – C. 7898.

8. Matthews DR, Hosker JP, Rudenski AS, et al. Homeostasis model assessment: insulin resistance and β-cell function from fasting plasma glucose and insulin concentrations in man. Diabetologia. 1985;28(7):412-419.

9. Rico-Fontalvo J. et al. Inflammatory and lipotoxicity mechanisms in obesity related CKD //Frontiers in Nephrology. – 2025. – T. 5. – C. 1684004.